

The Role of Architecture in the Elastic Response of Semiflexible Polymer and Fiber Networks

Claus Heussinger and Erwin Frey

Arnold Sommerfeld Center for Theoretical Physics and CeNS,

Department of Physics, Ludwig-Maximilians-Universität München,

Theresienstrasse 37, D-80333 München, Germany and

Hahn-Meitner-Institut, Glienicker Strasse 100, D-14109 Berlin, Germany

(Dated: April 10, 2019)

We study the elasticity of cross-linked networks of thermally fluctuating stiff polymers. As compared to their purely mechanical counterparts, it is shown that these thermal networks have a qualitatively different elastic response. By accounting for the entropic origin of the single-polymer elasticity, the networks acquire a strong susceptibility to polydispersity and structural randomness that is completely absent in athermal models. In extensive numerical studies we systematically vary the architecture of the networks and identify a wealth of phenomena that clearly show the strong dependence of the emergent macroscopic moduli on the underlying mesoscopic network structure. In particular, we highlight the importance of the total polymer length that to a large extent controls the elastic response of the network, surprisingly, even in parameter regions where it does not enter the macroscopic moduli explicitly. We provide theoretical scaling arguments to relate the observed macroscopic elasticity to the physical mechanisms on the microscopic and the mesoscopic scale.

PACS numbers: 87.16.Ka, 62.20.Dc, 82.35.Pq

I. INTRODUCTION

A one-component isotropic solution of semiflexible polymers shows complex viscoelastic properties and represents an interesting model-system being studied for many years. One of the main quantities of interest is the plateau value of the shear modulus found at intermediate timescales where single polymer bending fluctuations are equilibrated, yet center of mass motion is negligible. The generally accepted theory for the concentration dependence of the plateau modulus is based on the free energy change of confining a polymer to a tube [1, 2, 3], the diameter of which is a consequence of the structural organization of the tubes in the form of a random assembly of cylinders [4]. Realizations of this packing architecture have recently been achieved in simulations [5, 6] as well as (macroscopic) experiments [7].

Upon the addition of cross-linking agents or other regulating proteins one can induce structural changes to modify the network architecture in many ways. There have been attempts to describe the phase-diagram of these systems [8, 9], the detailed mechanisms that lead to a particular structure, however, are far from being understood. In general, there will be a complex interplay of polymer kinetics, thermal fluctuations and chemical as well as mechanical properties of the polymers and the cross-linking agents yielding a particular architecture relevant for a given physical situation.

A complementary approach is to neglect the “dynamic” aspects of the network, which is constantly changing its structure, and to concentrate on a “static” architecture and its effect on the macroscopic elasticity.

In the (structural) engineering community, for example, it is of tantamount importance to analyze the architecture of structures made of beams or trusses. A com-

mon way to take advantage of the reduced weight compared to the bulk material without suffering from a loss of stiffness is a triangulation of the basic cells. This eliminates the soft bending modes of the beams and makes it possible to construct huge cantilever bridges like that over the Firth of Forth in Scotland or towers like Eiffel’s tower in Paris. Since the rigidity of these structures is not due to the individual beam but to a non-local back-coupling effect induced by the architecture of the network, the triangulation is therefore one example on how cooperativity among the building blocks may be possible.

To address this question of cooperativity in the context of the elasticity of cross-linked stiff polymer networks we will concentrate in the following on the two generic structures of *cellular* and *fibrous* networks (see Fig.1) that may serve as reference systems for the classification of real polymer networks. The goal will be to identify possible mechanisms of how the particular structure couples to the properties of the individual polymers to effectuate the macroscopic elasticity of the system.

The paper is organized as follows. In Sect.II we motivate our approach to the modeling of thermally fluctuating networks of stiff polymers. This will lead us to the definition of effective elastic properties of the “polymer segments” that constitute the elementary building blocks of the network. In Sect.III and IV these polymer segments are assembled into cellular and fibrous networks, respectively. The macroscopic elastic constants of these structures are calculated and related to the particular architectural features. Finally, in Sect.V we present our main conclusions and hint at implications for possible experiments.

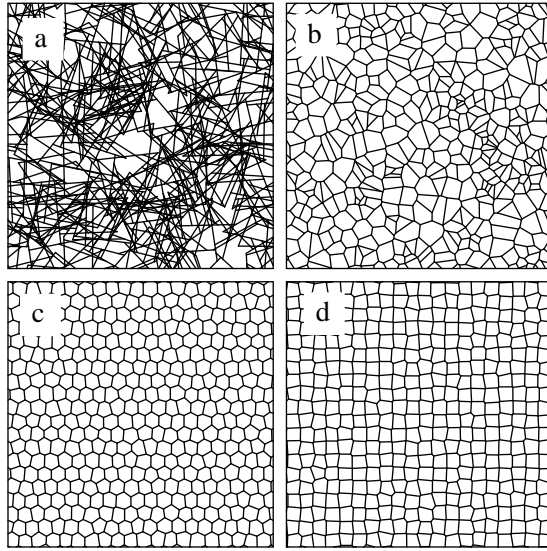


FIG. 1: Illustration of the different architectures of (a) fibrous and (b-d) cellular materials. While (a) and (b) are random structures generated by Poisson point processes, (c) and (d) are quite regular networks based on honeycomb and square lattices, respectively.

II. MODEL DEFINITION

To study the elastic properties of thermally fluctuating cross-linked stiff polymer networks we calculate numerically the low frequency shear modulus. Using the above mentioned time-scale separation between the fast bending fluctuations of the single polymer and their very slow center of mass motion, we adopt a description of the system in the spirit of a Born-Oppenheimer approximation. This neglects the fluctuations of the “slow variables”, the cross-link positions, while assuming the “fast” polymer degrees of freedom to be equilibrated at all times.

Macroscopic quantities will then depend parametrically on the set of cross-link variables. The shear modulus can be calculated by minimization of the internal energy respecting the constraints of a given macroscopic shear strain γ .

By holding the cross-link coordinates fixed, the energy of the system can be written as a sum

$$E = \sum_{\alpha} e(\mathbf{x}^{\alpha} - \mathbf{x}_0^{\alpha}), \quad (1)$$

over contributions from individual polymer segments α , each of which connects a given pair of cross-links. The single segment energy e depends on the generalized “displacement-vector” $\mathbf{x}^{\alpha} - \mathbf{x}_0^{\alpha}$, which incorporates the degrees of freedom of both defining cross-links. The six components of a vector $\delta\mathbf{x} = (\mathbf{u}_0, \theta_0, \mathbf{u}_l, \theta_l)$ are in-plane displacements $\mathbf{u}_{0,l}$ and rotations $\theta_{0,l}$ at both ends 0, l of the segment (see Fig.2). Note, that the additional vari-

able of cross-link rotation sets our system apart from bond-bending and related models where only translational degrees of freedom are accounted for.

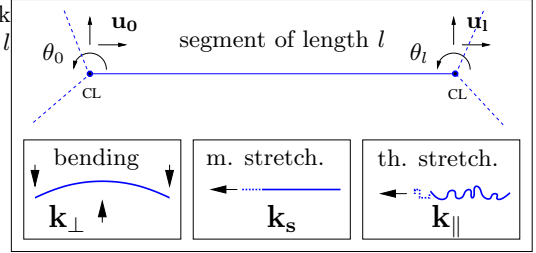


FIG. 2: Illustration of a polymer segment of length l and its connection to the network at the cross-links (CL). The three degrees of freedom at each cross-link are denoted by \mathbf{u} and θ , respectively. Identification of the three possible modes of deformation and their stiffnesses k_{\perp} , k_s and k_{\parallel} as defined in the text.

To leading order, in linear elasticity, the single polymer quantity e is a quadratic function of its coordinates

$$e(\mathbf{x}) = \frac{1}{2} \sum_{ij} K_{ij}(l) x_i x_j, \quad (2)$$

which defines the “stiffness matrix” K_{ij} (spring constants) of the polymer strand.

The matrix elements are well established in models of classical beams of radius r and bending stiffness κ . It turns out that the response of a beam of length l_s is sufficiently characterized already by two of the elements

$$k_s(l_s) = 4\kappa/l_s r^2, \quad k_{\perp}(l_s) = 3\kappa/l_s^3, \quad (3)$$

relating to stretching (s) and bending (\perp) deformations, respectively (see Appendix A for a derivation of the complete matrix). Due to their small aspect ratios $r/l_s \ll 1$ such slender rods are highly anisotropic and much softer in bending than in stretching.

Here, we consider thermally fluctuating stiff polymers immersed in a heat bath of solvent molecules. In these systems, the effects of temperature on the elastic properties of the polymer can be quantified by defining the persistence length l_p as the ratio of bending to thermal energy $l_p = \kappa/k_B T$. With this definition we assume in addition to the enthalpic stiffness of the classical beam an entropic contribution

$$k_{\parallel}(l_s) = \zeta \kappa \frac{l_p}{l_s^4}, \quad (4)$$

to the polymer’s stretching compliance that can be calculated with the wormlike chain model. The prefactor ζ depends on the specific boundary conditions chosen at the ends of the polymer segment. Its value can be absorbed in the persistence length, and therefore only quantitatively affects the results. To avoid a large numerical offset with respect to Eq.(3), we have chosen $\zeta = 6$, which

resembles a worm-like chain clamped at one end [10]. Having two longitudinal deformation modes the effective stretching stiffness is equivalent to a serial connection of the “springs” k_s and k_{\parallel} .

As one can see, at a given temperature T there are two length scales characterizing the material properties of the polymers, the radius r and the persistence length l_p . Typical biological polymers are characterized by a ratio $R = l_p/r \gg 1$. F-actin, for example, a key component of the cytoskeleton has $R = O(10^4)$ ($r = 5\text{nm}$, $l_p = 17\mu\text{m}$), while microtubules, most important for cell-division and intra-cellular transport, have an even larger $R = O(10^6)$. For specificity, we require in the following a constant $R = 1.5 \cdot 10^4$, the precise value, however, is irrelevant if one is interested only in the thermal response where the radius does not enter and $k_s \rightarrow \infty$. Occasionally, we will perform this limit to highlight features that are independent of the mechanical stretching response. On the other hand, the location of the cross-over point, where the mechanical stretching becomes relevant, does indeed depend on the choice of R . By definition it determines the relative magnitude of the two stretching compliances k_s and k_{\parallel} .

This completes the specification on the microscopic scale of the elastic properties of the single polymer segments. We now proceed to assemble the segments into networks of varying architecture to identify the physical principles which determine the elastic response on the macroscopic scale.

To determine the elastic shear modulus, we apply a small shear strain of $\gamma = 0.01$ to stay in the regime of linear elasticity and use periodic boundary conditions on all four sides of the simulation box. The numerical procedure is performed with the commercially available finite element solver MSC.MARC. The results will be complemented by scaling arguments.

We will find that in *regular cellular architectures*, to be discussed next, macroscopic elasticity can trivially be explained by the microscopic constitutive laws given in terms of the stiffness matrix \mathbf{K} . In sufficiently *random cellular systems*, however, this picture is changed. The macroscopic response takes up nontrivial features that cannot be explained by single polymer elasticity. In *fibrous architectures*, subject of Sect.IV, we will find this anomalous elasticity again but in more striking form.

III. CELLULAR ARCHITECTURE

A cellular structure is most conveniently constructed from a Voronoi tesselation of a distribution of points which may either be chosen regularly or by some random process. With each point we associate a Voronoi cell that is defined to enclose that region in space which is closer to the given point than to any of its neighbours. This procedure is equivalent to the Wigner-Seitz construction known from solid-state physics. In three dimensions the elastic elements are defined to be the lines of intersec-

tion of two neighbouring cell walls, while in two dimensions (see Fig.1) they are represented by the cell walls themselves. We will call these elastic building blocks of the network *polymer segments* and associate to them the material properties, respectively the stiffness matrix \mathbf{K} , introduced in the preceding section. By its definition, a segment spans the distance between two vertices and is therefore “end-linked” with the rest of network.

Depending on the spatial distribution of Voronoi points there will also be a distribution $P(l_s)$ of segment lengths l_s . Only in regular structures, for example the (anisotropic) two-dimensional honeycomb structure, this distribution will degenerate into one (or several) delta-function peaks.

The first moment of this distribution, the average segment length \bar{l}_s , is naturally the most important quantity to describe the geometrical aspects of a cellular structure. In $d = 2, 3$ dimensions this “mesh-size” may be reparametrized in terms of the density ρ as

$$\bar{l}_s \propto \rho^{-1/(d-1)}, \quad (5)$$

where we defined ρ as the total polymer length per system size. In experimental work it is sometimes easier to control the monomer concentration c , which can be found as $rc \propto \rho$, where the radius r is assumed proportional to the monomer size.

A. Mechanical Behaviour: Beams

In the engineering literature the cellular structures defined above are well known as foams and are ubiquitous in nature and many areas of technology. Examples range from liquid foams and froths well known from drinks or household detergents, to plastic and metallic foams used for insulation or shock absorption [11, 12]. It is well known that naturally occurring foams have to obey Plateau’s laws to reach an equilibrium state. We do not require these laws to hold in the following, since we are interested in the dependence of elastic properties on the architectural features in general, and not in the specific details of the dynamic properties of foams.

For purely mechanical cellular foams the only material length scale is the radius r of the cross-section. By identifying κ/\bar{l}_s as an energy scale, we can use dimensional analysis to write the shear modulus G as

$$G = \frac{\kappa}{\bar{l}_s^{d+1}} g(r/\bar{l}_s), \quad (6)$$

where the occurrence of the spatial dimension d highlights the fact that the modulus has units of an energy density. In writing this, we have not made explicit the dependence on the higher moments of the probability distribution P . As will become clear below, these can be used to characterize the randomness of the structure and will be considered separately. If one defines force-constants at the scale of the average mesh-size

$$\bar{k}_{\perp} \simeq \kappa/\bar{l}_s^3, \quad \bar{k}_s \simeq \kappa/\bar{l}_s r^2, \quad (7)$$

the scaling variable can alternatively be written as $r/\bar{l}_s \simeq \sqrt{\bar{k}_\perp/k_s}$ and therefore characterizes the relative stiffness of the bending to the stretching mode.

B. Regular Structures and Affine Models

Restricting our attention for the moment to regular structures, macroscopic elasticity can already be understood by considering the response of a single cell [12, 13, 14]. In these systems it seems reasonable that local stresses acting on an individual cell are the same as those applied on the macroscopic scale. In other words, the local deformation δ of a cell with linear dimension \bar{l}_s follows the macroscopic strain γ in an *affine way* such that it scales as $\delta \propto \gamma \bar{l}_s$. With this assumption the scaling function can be calculated [13] and one generically finds for the modulus

$$G_{\text{aff}}^{-1} = \bar{l}_s^{d-2} (a \bar{k}_\perp^{-1} + b \bar{k}_s^{-1}), \quad (8)$$

where the details of the particular structure may enter the numbers a and b in an involved way. The important conclusion to be drawn is that the deformation modes act as if they were springs connected in series. For slender beams with $r \ll \bar{l}_s$ the bending mode is softer than the stretching mode and therefore dominates the modulus – mechanical foams are *bending dominated*.

While we argue here that the modulus in Eq.(8) represents the generic case, there may be special cases were the prefactors a or b are suppressed by the specific choice of the unit cell. The triangulated network is one example where $a = 0$ and the bending mode is suppressed. Below we will encounter another example when studying the square lattice. For these systems the special geometry of the unit cell, or more generally, the local architecture has to be taken into account. This is indeed the main focus of this article.

On the other hand, by assuming affine displacements no cooperativity between the elastic responses of neighboring cells can be possible. The macroscopic modulus G directly reflects the elastic properties of the single cell. The local geometry is being hidden in the prefactors a and b , while the effect of the assembled structure can simply be predicted by counting the numbers of cells.

C. Cell Polydispersity

We have tested the validity of the affine model in a simple two-dimensional cellular structure with varying degree of randomness. We have taken the seeds for a Voronoi construction of a regular, honeycomb lattice structure and randomly displaced them with a uniform probability distribution of width Δ . The influence of randomness on the elastic properties of mechanical (non-fluctuating) foams has been studied extensively by various authors [15, 16, 17]. Here, we also include effects

from thermal fluctuations such that the response of a polymer segment is characterized by three deformation modes with stiffnesses k_s , k_{\parallel} and k_{\perp} , respectively. The affine prediction for the modulus of this system ($d = 2$) can be inferred from Eq.(8). By defining

$$\bar{k}_{\parallel} \simeq \kappa l_p / \bar{l}_s^4, \quad (9)$$

and substituting $\bar{k}_s^{-1} \rightarrow \bar{k}_s^{-1} + \bar{k}_{\parallel}^{-1}$ one finds for the modulus

$$G_{\text{aff}}^{-1} = \frac{\bar{l}_s^3}{\kappa} \left(a + b \left(\frac{R \bar{l}_s}{l_p} \right)^{-2} + c \frac{\bar{l}_s}{l_p} \right) = \bar{k}_{\perp}^{-1} g(l_p / \bar{l}_s), \quad (10)$$

where we have inserted Eqs.(7) and (9) and used the relation $R = l_p/r$. This has to be compared with the actual results of our numerical analysis in Fig.3. The normalized shear modulus $G \bar{l}_s^3 / \kappa$ is shown as a function of persistence length $y = l_p / \bar{l}_s$ expressed in units of the average segment length. The curves correspond to varying degrees of randomness.

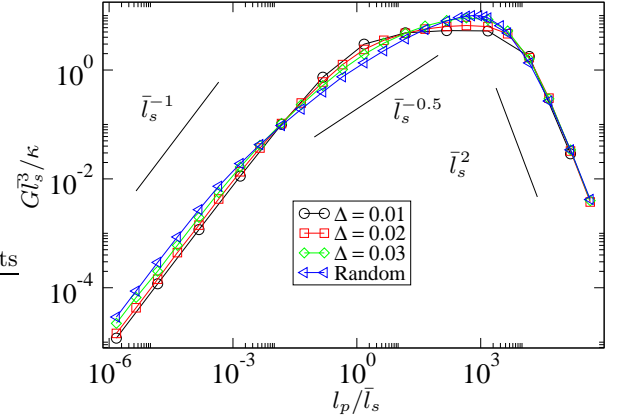


FIG. 3: Shear modulus $G \bar{l}_s^3 / \kappa$ as a function of l_p / \bar{l}_s for a 2d honeycomb foam structure with varying degree of randomness Δ (defined as the maximum deviation of a given (Voronoi) seed from the lattice structure). The blue curve (“random”) corresponds to a “maximally” random foam generated from a Poisson point process (the lines are guides to the eye).

As a result, regular networks (black curve, circles) characterized by a single mesh-size \bar{l}_s indeed display the scaling behaviour indicated in Eq.(10). For mesh-sizes much larger than the persistence length $\bar{l}_s \gg l_p$ the network deforms by pulling of thermal undulations and $G \propto \bar{k}_{\perp} \propto \bar{l}_s^{-4}$ (left part of Fig.3). Decreasing the mesh-size beyond $\bar{l}_s \approx r$ stretching of the polymer backbone dominates the modulus $G \propto \bar{k}_s \propto \bar{l}_s^{-1}$ (right part of Fig.3). The physically relevant situation for the study of stiff polymers, however, corresponds to the intermediate regime, where the mesh-size is much smaller than the persistence length much still larger than the polymer radius $l_p \gg \bar{l}_s \gg r$. In this regime, most of the energy is stored in the bending modes leading to $G \propto \bar{k}_{\perp} \propto \bar{l}_s^{-3}$

and the plateau region in Fig.3. Typical actin networks with $l_p = 17\mu\text{m}$ and $r = 4\text{nm}$ may have mesh-sizes in the submicron range $\bar{l}_s \approx 100\text{nm}$.

Increasing the level of randomness the presence of the additional variable Δ spoils the scaling property. The power law regimes gradually shrink and the cross-over regions increase in size. While the mechanical stretching regime is hardly affected by the randomness at all, this effect is most pronounced in the cross-over from the bending to the thermal stretching dominated regime. The physically most relevant intermediate plateau regime disappears completely and shows strong amplitude modulations.

We have also generated random foams by Voronoi tessellation of a Poisson point process (blue curve, left triangles). For these “maximally random foams” one could rather use an expression $G \propto \bar{l}_s^{-7/2}$ to characterize the modulus at these intermediate parameter values. At this point this is only an empirical observation. However, we will see later in the context of the fibrous architecture how this exponent can be determined from a subtle interplay between a length-dependent force constant $k_{\parallel}(l_s)$ and the presence of a wide range of segment lengths l_s .

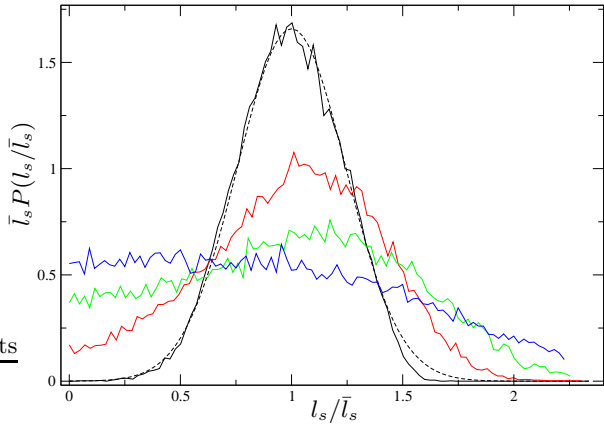


FIG. 4: Distribution of segment lengths for the same systems as studied in Fig.3. The dashed line is a fit to a Gaussian probability distribution.

Looking at Fig.4 one recognizes that deviations from the scaling form presented in Eq.(10) are indeed intimately connected to a broadening of the segment length distribution. The regular structure can very well be described by a Gaussian centered around the average mesh-size \bar{l}_s (dashed line in Fig.4). Random foams, on the contrary, display significantly broader distributions and even have non-negligible weight on very small segments.

We will see below that the different response to randomness in the thermal and the mechanical stretching regimes can be traced back to the unusually strong length dependence of the entropic stretching stiffness $k_{\parallel} \propto l_s^{-4}$ as compared to $k_s \propto l_s^{-1}$. This leads to the breakdown of the affine model whenever there is a sufficiently broad distribution of segment lengths. Thermal networks are

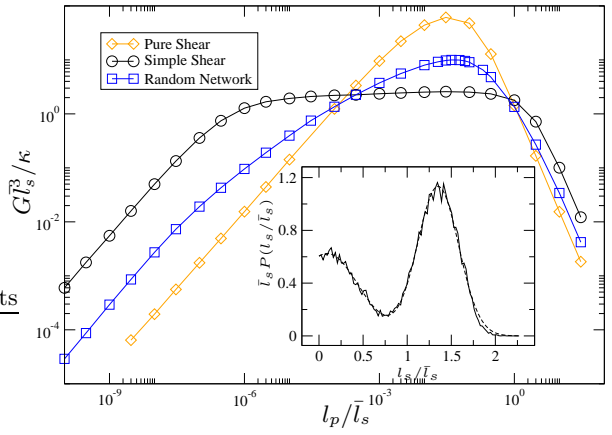


FIG. 5: The two different shear moduli for the slightly randomized square lattice as shown in Fig.1. Inset: Distribution of segment lengths for the same network. The dashed line is a fit to a sum of two Gaussians centered around $l_s/\bar{l}_s = 1.35$ and $l_s/\bar{l}_s = 0.092$.

thus inherently more sensitive to elements of randomness than purely mechanical systems.

For now it will be illuminating to consider another lattice structure as a basis for our foam model (see Fig. 1). By placing the Voronoi points on a slightly randomized square lattice one can generate a foam with a bimodal segment length distribution (see inset Fig.5). One just has to realize that a generic foam structure generated by Voronoi tessellation has only three-fold connected vertices, while they are four-fold connected in the square network. A small amount of randomness therefore induces a bifurcation of a four-fold vertex into a short segment with three-fold connected vertices at its ends. Unlike the honeycomb foam, the resulting structure is elastically anisotropic and has 3 distinct moduli [18]. In addition to the bulk modulus there are two shear moduli corresponding to simple and pure shear deformations. These two (together with the isotropic shear modulus of the Poisson foam) are shown in Fig.5.

Pure shear leads to deformations along the main axis of symmetry of the unit squares and thus to stretching of the elements. The bending regime is therefore strongly suppressed. On the other hand, simple shear deforms the squares along their diagonals and thus favours the bending mode. Only when the stretching energy stored in the small segments $w_{\parallel} = k_{\parallel}(l_1)\delta_{\text{aff}}(l_1)^2 \propto l_p/l_1^2$ equals the bending energy in the average segment $w_{\perp} = k_{\perp}(\bar{l}_s)\delta_{\text{aff}}(\bar{l}_s)^2 \propto \bar{l}_s^{-1}$ does the system cross-over to a stretching dominated network. Noting (from the inset of Fig.5) that $l_1 \approx \bar{l}_s/10$ we find that this happens when $l_p \approx 10^{-2}\bar{l}_s$ in accord with Fig.5. It is interesting to see that the network loses its anisotropy at the two points $\bar{l}_s = l_p$ and $\bar{l}_s = r$, where the modulus takes the same value as that of the Poisson foam. This derives from the fact that the stiffness of the average polymer segments is isotropic at these parameter values and either $\bar{k}_{\parallel} \approx \bar{k}_{\perp}$

or $\bar{k}_s \approx \bar{k}_\perp$. Comparing absolute values we find that the shear modulus in the thermal regime, strongly influenced by the presence of the small segments, can vary orders of magnitude while the mechanical stretching regime is hardly affected at all.

To conclude this section we emphasize once again that polydispersity in the segment lengths can have strong effects on the macroscopic elasticity of a cellular polymer network. It can lead to modifications of the scaling properties, as we have found in the most random foams, as well as to quantitative changes of the modulus by several orders of magnitude as in the anisotropic square structure. As a consequence, experiments which are limited to restricted parameter windows would most likely measure effective exponents that lie in between the extremal values given by pure stretching and bending. One, therefore, has to be cautious interpreting experimental data within the context of the foam-model, without the knowledge of the polydispersity of the structure.

IV. FIBROUS ARCHITECTURE

Looking at pictures of cross-linked actin networks reconstituted *in vitro* [19, 20] one might wonder whether a description in terms of a cellular architecture is actually relevant for these systems at all. Besides having a strong polydispersity in cell sizes, real polymer networks seem to have a hierarchical architecture that allows for smaller cells to be generated within larger cells within even larger cells. On the contrary, foams only have one of these hierarchies (see Fig.1). What is more, cellular structures do not account for the effects of the polymer length l_f , which constitutes an additional mesoscopic scale in the problem.

In the following we want to quantify the effects of the polydispersity in connection with the length scale l_f by studying the elastic properties of a generic two-dimensional fibrous structure which is defined as follows. N anisotropic elastic elements, geometrically represented by straight lines of length l_f , are placed on a plane of area $A = L^2$ such that both position and orientation of the elements are uniformly random distributed. At any intersection a permanent crosslink with zero extensibility is generated. This constrains the relative translational motion of the two filaments. For the rotational degree of freedom one may introduce an energy contribution $W_{rot} = m(\phi - \phi_0)^2$ for the change of relative cross-link angles ϕ from their initial values ϕ_0 . We restrict ourselves to study of the two limiting cases, where the potential is either soft ($m \rightarrow 0$) and therefore allows for free relative rotations of the filaments (free hinges), or infinitely stiff ($m \rightarrow \infty$) and inhibits any change of the angles at the cross-links (fixed angles).

The remaining elastic building blocks of the network, the *polymer segments*, span the distance between two neighbouring cross-links on the same polymer. Their length can be shown to follow an exponential distribu-

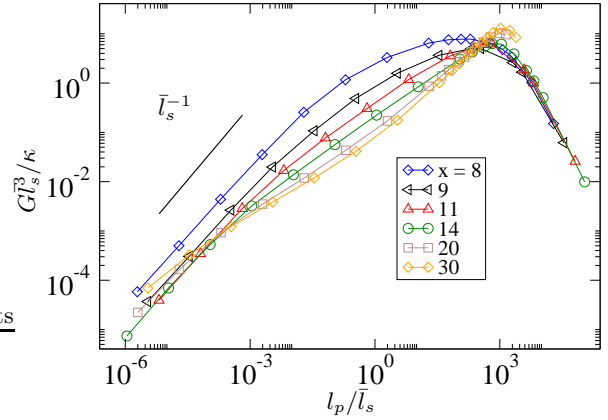


FIG. 6: Scaling function g as a function of $y = l_p/\bar{l}_s$ for various $x = l_f/l_s \leq 30$;

tion [21]

$$P(l_s) = \bar{l}_s^{-1} e^{-l_s/\bar{l}_s}. \quad (11)$$

The mean value \bar{l}_s is given in terms of the density $\rho = Nl/A$ as

$$\bar{l}_s = \pi/2\rho, \quad (12)$$

which is a realization of Eq.(5). On average there are, thus, $l_f/\bar{l}_s \approx l_f\rho$ segments per polymer. The simplicity of this network, which has only one structural parameter ρ , makes it an ideal candidate to obtain physical insight into the relation between architecture and elastic properties of the constituents. This model has frequently been used to study the elastic and brittle properties of athermal paper sheets [22, 23, 24, 25]. In the context of biological networks of stiff polymers it has been introduced in [26] and recently studied by various authors [27, 28, 29]. In all this work, however, the elastic properties of the polymers are modeled by the classical theory of Euler-Bernoulli beams. Here, we concentrate on the effects of thermal fluctuations, a brief account of which we have published recently [30].

A. Simulation Results

In Figs. 6 and 7 the results of our simulations are shown for fibrous networks with a varying number x of cross-links per polymer. The axes are the same as in previous plots. Short fibers with few cross-links, corresponding to low densities are depicted in Fig. 6, long fibers or high densities in Fig. 7. In both figures we find a regime at large values of the persistence length l_p/\bar{l}_s (right part of the plot) where the dimensionless shear modulus decreases as $G \propto l_p^{-2} \propto r^{-2}$. This corresponds to a purely mechanical stretching regime where $G \propto \bar{k}_s$ consistent with the mean-field picture of Eq.(10) [22, 26, 27, 28].

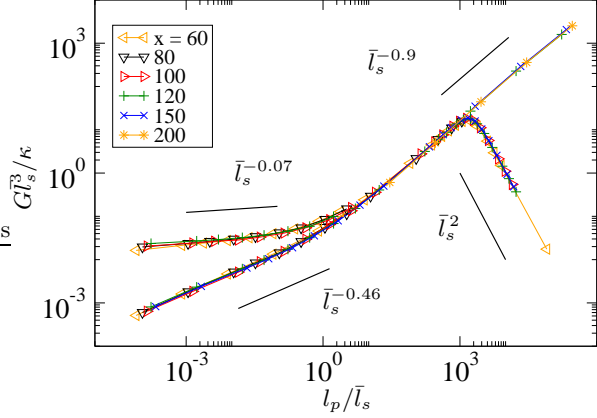


FIG. 7: Scaling function g as a function of $y = l_p/\bar{l}_s$ for various $x = l_f/\bar{l}_s \geq 60$; The two branches in the cross-link dominated regime ($y \ll 1$) correspond to freely hinged (CL_{free}) or fixed (CL_{fixed}) cross-link angles, respectively. For $y \gg 1$ one encounters a universal thermal regime (U) independent of the cross-link properties as well as a mechanical regime (M).

Our main interest, however, lies in the regime of small l_p/\bar{l}_s , where the persistence length is small enough for thermal fluctuations to become relevant. In this regime one may safely neglect the mechanical stretching stiffness and set $k_s \rightarrow \infty$. Then, dimensional analysis requires

$$G = \frac{\kappa}{l_s^3} g(x, y), \quad (13)$$

where we have introduced the scaling variables

$$x = l_f/\bar{l}_s \simeq l_f \rho, \quad y = l_p/\bar{l}_s \simeq l_p \rho. \quad (14)$$

Comparing to Eq.(6) we have an additional argument in the scaling function g , the polymer length $x = l_f/\bar{l}_s$. This purely geometrical variable counts the number of crosslinks (or alternatively: segments) per filament. The second argument can be written in the alternative form $y \simeq \bar{k}_\parallel/k_\perp$ and characterizes the relative stiffness of stretching and bending mode for a typical segment.

From Fig. 6 one infers that for *low densities* $g = yf(x)$, implying for the modulus $G = \bar{k}_\parallel f(\rho l_f)$. This linear dependence on the “pre-averaged” stretching compliance \bar{k}_\parallel hints at an entropic stretching dominated regime similar to that found in the cellular structures discussed above. This regime has been suggested in [29], where a scaling argument is developed relying on the affine assumption borrowed from the mechanical stretching regime. Our analysis shows that the domain of validity of this linear regime is extremely narrow and confined to short filaments $x \leq 20$ and persistence lengths $y \ll 1$. What is more, due to the non-trivial density-dependence expressed through the function $f(x)$, the modulus does not even display power-law behaviour in density. Instead, we find that the modulus shows complex dependence on its variables and develops a dip in the intermediate parameter region. The strong variation of the modulus in

this regime may actually be observable in networks of F-actin, where the ratio of persistence-length to mesh-size $l_p/\bar{l}_s \approx 10 - 100$.

For *medium and high densities* Fig. 7 shows non-trivial scaling regimes where the scaling function g becomes independent of x and therefore of the filament length l_f . It exhibits power law behavior $g \propto y^z$ with non-trivial fractional exponents $z = 0.46(0.07)$ and $z = 0.9$ for small and large values of y , respectively. In the figure one can distinguish four branches that belong to different realizations of the network. While branch M (mechanical regime, $G \propto \bar{k}_s$) has been discussed already, the remaining three are obtained by setting $k_s \rightarrow \infty$. The two branches found at small values $y \ll 1$ relate to networks where the cross-link angles are either free to vary (CL_{free}) or are perfectly fixed to their initial values (CL_{fixed}), respectively. We will call this regime cross-link dominated since tuning the cross-link properties may have strong effects on the elastic modulus by driving the system from one branch towards the other. Both branches merge at $y \approx 1$ where we enter a universal regime (branch U) which is completely independent of the elasticity of the cross-links and which therefore is “filament dominated”.

In all cases, the modulus can be written as a generalized geometric average

$$G \propto \bar{k}_\perp^{1-z} \bar{k}_\parallel^z, \quad (15)$$

which has to be contrasted with Eq.(10), where bending and stretching modes are assumed to superimpose linearly. There, the system is described either by $z = 0$, if bending dominates, or by $z = 1$ if stretching is the main deformation mode. Different values, as found here, cannot be described by the mean-field approach presented there. The assumption of affine deformations applied on the level of the polymer segments (or the cell size) necessarily has to fail.

This will become especially clear in the following section, where we review the application of affine theories to fibrous architectures. We will illustrate its failure and highlight the physical principles involved. To go beyond we will introduce a model that accounts for the spatial distribution of cross-links along the backbone of a *typical polymer filament* instead of just considering a single *typical polymer segment*. This new approach will allow us to understand all the features of the macroscopic elasticity encountered in Fig.7.

B. Affine Models in Fibrous Architectures

In some of the earlier approaches to describe the elastic moduli of stiff polymer networks the assumption of affine deformations has been applied on the level of the average segment characterized by “pre-averaged” response coefficients $\langle k(l_s) \rangle \rightarrow \bar{k} = k(\bar{l}_s)$ introduced in Eqs.(7) and (9). The characteristic fibrous structure of stiff polymer networks is not accounted for and effectively substituted by a highly regular cellular structure. The modulus in

the thermal regime is then obtained simply by replacing in Eq.(8) the mechanical stretching response \bar{k}_s with its thermal counterpart \bar{k}_{\parallel} . Several variants of this model have been considered in the literature [10, 31, 32] that only differ in the specific (ad hoc) choice of the prefactors a, b . Especially the stretching dominated model [31] (setting $a = 0$ in Eq.(8)) with a modulus depending on density as

$$G_{\parallel} \sim \rho^{(2+d)/(d-1)}, \quad (16)$$

as well as its extensions to nonlinear elasticity [33], have widely been used to fit experimental data for the plateau modulus in cross-linked F-actin networks [19, 20, 34]. Despite this apparent success, it is not clear a priori why in the parameter regime of interest the mesh-work should deform by the stretching of bonds when bending is by far the softer mode ($\bar{k}_{\parallel}/\bar{k}_{\perp} \simeq l_p/\bar{l}_s \gg 1$). In general, such a regime can only occur if the specific architecture suppresses the soft bending modes as in the triangulated structure with its highly coordinated vertices. A second approach seems to repair this deficiency by setting in Eq.(8) $b = 0$. The modulus in this theory

$$G_{\perp} \sim \rho^{(1+d)/(d-1)}, \quad (17)$$

only differs by a factor of $\rho^{1/(d-1)}$ from the stretching dominated modulus of Eq.(16). However, neither theory provides justification for neglecting the effects of the polydispersity in the fibrous system. In fact, if one extends the approach to include the distribution of segment lengths, such theories necessarily have to fail, as we will explain in the next section.

C. Effects of the Segment Length Distribution

To understand the origin of this failure consider an affine deformation field $\delta_{\text{aff}} \propto \gamma l_s$ being applied to a random network of stiff polymers with a distribution $P(l_s)$ of segment lengths l_s . The axial forces f_{\parallel} generated by this deformation field can simply be calculated by multiplying the deformation with the stretching stiffness of the segment

$$f_{\parallel} = k_{\parallel} \delta_{\text{aff}} \simeq \kappa l_p \gamma / l_s^3. \quad (18)$$

In contrast to the purely mechanical situation, where the axial force $f_s = k_s \delta_{\text{aff}} \simeq \kappa \gamma / r^2$ is independent of length, f_{\parallel} strongly increases with shortening the segment length. This implies that, in general, two neighboring segments on the same filament produce a net force at their common node that has to be taken up by the crossing filament. There, it leads to additional deformations that eventually destroy the affine order.

One can calculate the probability distribution Q for residual forces by summing over all network configurations that produce a given force δf . This involves the two-point probability $P(l_1, l_2)$ of finding neighbouring segments with lengths l_1 and l_2 , respectively. In the special

case of the random network considered here, there are no correlations between neighbouring segment lengths such that the distribution factorizes. We therefore have to evaluate the formula

$$Q(\delta f) = \int_{l_1} P(l_1) \int_{l_2} P(l_2) \delta(|f_{\parallel}(l_1) - f_{\parallel}(l_2)| - \delta f), \quad (19)$$

which can be performed by substituting $f_{\parallel} \propto l_s^{-3}$ taken from Eq.(18). This inverse relationship between forces and segment lengths translates the weight of the probability distribution $P_0 = P(l_s \rightarrow 0) \neq 0$ at small segment lengths into polynomial (fat) tails of the corresponding distribution of residual forces

$$Q(\delta f \rightarrow \infty) \propto \delta f^{-4/3} P_0, \quad (20)$$

which has a diverging mean value. The exponent can readily be derived from evaluating the integral measure $df \propto l^{-4} dl \propto f^{-4/3} dl$. As a consequence there are always residual forces high enough to cause significant bending of the crossing filament. Hence we conclude that an affine deformation field is unstable and that the system can easily lower its energy by redistributing the stresses to relieve shorter segments and remove the tails of the residual force distribution $Q(\delta f)$.

Even though we have evaluated Eq.(19) for the special case of an exponential segment length distribution Eq.(11), it is important to note, that the discovered susceptibility is not a special feature of the fibrous architecture, but applies to any polymer network with a broad distribution of segment lengths. Due to the strong length dependence of $k_{\parallel}(l_s)$ the thermal response is highly sensitive to even small polydispersity as we have seen already in the random cellular network of Sect.III C. On the contrary, these effects are completely absent in purely mechanical models, where the distribution $Q(\delta f)$ degenerates into a delta-function peak at the value $\delta f = 0$, and explains the robustness of these regimes to randomness.

If we want to include the effects of randomness into a microscopic theory we cannot naively apply the conventional picture of affine deformations on the scale of the single segment. This can safely be done only in highly ordered structures like regular cellular materials. Instead, we have to adopt a description of the deformations on the larger scale of the complete polymer. We therefore consider in what follows a *typical polymer filament*, which is composed of a sequence of segments drawn from the distribution $P(l_s)$. To describe the elastic properties correctly, we will also have to consider the connections of the polymer to the surrounding network matrix, in addition to the elastic properties of the segments themselves. We can employ this picture to explain the intricate scaling properties of the polymer network in all the parameter regimes displayed in Fig.7.

D. Cross-link dominated Regime

1. Freely hinged cross-links

We start with the description of the system in the parameter region $y \ll 1$ ($l_p \ll \bar{l}_s$), where the properties of the cross-links strongly influence the system's response. The idea will be to impose an artificial affine configuration on every segment and calculate the contribution to the elastic energy resulting from the relaxation out of this reference state. We restrict our attention for the moment to the case of free relative cross-link rotations (branch CL_{fixed}), because in this case the affine reference state is especially simple and contains stretching contributions only.

As explained above any deviation from the affine reference state, induced by relaxation of non-zero residual forces, will lead to additional deformations in the crossing filaments. If we assume that filaments are most likely oriented perpendicular to each other, then the induced non-affine deformations are mainly oriented transverse to the contour of the crossing filament and are therefore of bending character. The value of the exponent $z = 0.46$ supports this assumption and indicates that bending and stretching deformations in this regime contribute equally to the elastic energy even though the bending modes are very stiff ($\bar{k}_\parallel/\bar{k}_\perp \sim y \ll 1$). Therefore any relaxation of residual stretching forces, will be punished by high amounts of bending energy. Only the smallest segments on the polymer, corresponding to the outermost tails of the residual force distribution, will have sufficient energy to perturb the deformation field and relax to a state of lower strain.

In the following, we will assume that segments up to a critical length l_c – to be determined self-consistently – fully relax from their affine reference state to give all their energy to the neighboring segment on the crossing filament. The total energy of the polymer can then be calculated from segments with $l_s > l_c$ only. There are two contributions. First, a stretching energy

$$w_s(l_s) \simeq k_\parallel \delta_{\text{aff}}^2 \simeq \kappa \gamma^2 \frac{l_p}{l_s^2}, \quad (21)$$

from the imposed affine strain field $\delta_{\text{aff}} \propto \gamma l_s$. Second, a bending energy that is due to the relaxation of a neighboring segment on the crossing filament out of its affine reference state. This process requires that the segment of length \hat{l}_s moves the distance $\hat{\delta}_{\text{aff}} = \gamma \hat{l}_s$, which corresponds to its own affine deformation. The resulting bending energy

$$w_b(l_s) \simeq k_\perp \hat{\delta}_{\text{aff}}^2 \simeq \kappa \gamma^2 \frac{\hat{l}_s^2}{l_s^3}, \quad (22)$$

now depends on the length l_s of the segment under consideration as well as on the length \hat{l}_s of the neighbouring (relaxed) segment. As we have assumed above, the second contribution w_b only arises if the length \hat{l}_s is shorter

than the critical length l_c . The total deformation energy along the polymer is then obtained by adding both contributions and integrating over all segments that obey the conditions $l_s > l_c$ and $\hat{l}_s < l_c$,

$$W_{\text{pol}} \simeq (l_f \rho) \kappa \gamma^2 \int_{l_c}^{\infty} dl_s P(l_s) \left(\frac{l_p}{l_s^2} + l_s^{-3} \int_0^{l_c} d\hat{l}_s P(\hat{l}_s) \hat{l}_s^2 \right), \quad (23)$$

where the factor $l_f \rho$ in the front just counts the number of segments per polymer. For simplicity, we have not considered any dependence of the deformations on the orientation relative to the macroscopic strain field. This would only introduce additional numerical prefactors that are irrelevant for the scaling picture developed here. The integrations are reparametrized by introducing the non-dimensional variable $\lambda = \rho l_s$ such that we arrive at the expression

$$W_{\text{pol}} \simeq \kappa \gamma^2 l_f \rho^2 (\rho l_p / \lambda_c + \lambda_c), \quad (24)$$

where numerical constants have been dropped and $\lambda_c := \rho l_c \ll 1$ in the parameter range of interest. Minimizing with respect to λ_c gives the required expressions $\lambda_c^{\min} \simeq (l_p \rho)^{1/2}$ and $G \simeq W_{\text{pol}}^{\min} \cdot \rho / l_f \gamma^2 \simeq \kappa \rho^{7/2} l_p^{1/2}$, where we had to multiply the average polymer energy by the number-density of filaments ρ / l_f to arrive at an expression for the modulus. One may rewrite the result as

$$G \simeq \sqrt{\bar{k}_\perp \bar{k}_\parallel} \propto \bar{l}_s^{-7/2}, \quad (25)$$

where the correspondence with Eq.(15) is now obvious. Our theory yields a value $z = 1/2$ for the exponent in Eq.(15) which compares well with the measured value of $z = 0.46$.

It is important to realize that the derivation of the exponent does not make use of the precise form of the segment length distribution $P(l_s)$. In fact, there is no need to perform the integrations explicitly such that the conclusions are valid for a general class of functions that may even be slowly vanishing at zero segment length.

The non-trivial behavior of G observed in Fig. 7 can thus be explained by a length scale $l_c = \lambda_c \bar{l}_s \simeq \sqrt{\bar{l}_s l_p}$ below which the affinity of the deformation field breaks down. Recapitulating the results from the cellular networks in Fig.3, we observe that the same intermediate scaling behaviour of $G \propto \bar{l}_s^{-7/2}$ is found in both architectures. We have thus established the microscopic origin of the scaling law that derives from a continuous unloading of smaller segments driven by an interplay between segment length distribution and elastic properties of the single polymer.

In [30] we have communicated additional data that further validate this picture. There, we have shown that the stored elastic energy is shifted from small to large scales by increasing the value of l_p / \bar{l}_s . This is fully consistent with the assumption of a growing non-affinity scale l_c below which no energy is stored.

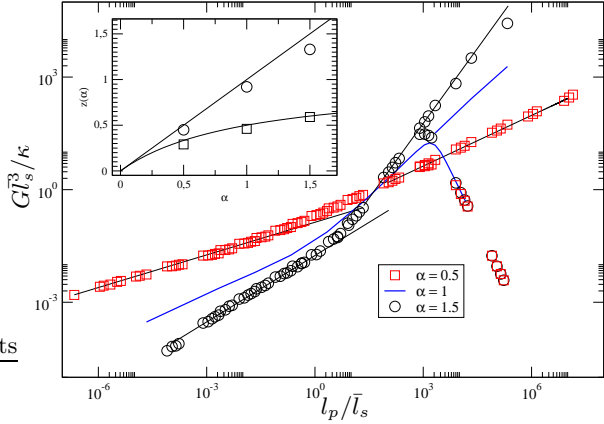


FIG. 8: Scaling function g as a function of $y = l_p/\bar{l}_s$; the different curves correspond to values of $\alpha = 0.5, 1, 1.5$. Inset: Power-law exponents z and analytical curves $z = \alpha$ and $z = \alpha/(1 + \alpha)$, respectively.

Furthermore, we have conducted simulations that assume a more general form for the stretching stiffness

$$k_{\parallel}(\alpha) = 6\kappa \frac{l_p^{\alpha}}{l_s^{3+\alpha}}, \quad (26)$$

which reduces to the original definition for $\alpha = 1$. The phenomenological exponent α allows us to extend our discussion to the broad class of systems for which k_{\parallel} is a monomial (with units energy per area) involving one additional material length l_p . Repeating the scaling theory for general values of α gives $z(\alpha) = \alpha/(1 + \alpha)$ which is verified by the results of the simulations presented in Fig.8.

2. Fixed Cross-link Angles

If we want to apply the same reasoning to the network with the fixed cross-link angles, we face the problem that even a perfectly affine displacement of all the cross-links induces some amount of bending of the segments, in addition to the usual contribution from the stretching deformations. While an affine strain γ would change all angles by an amount $\Delta\phi \propto \gamma$, due to the infinite rotational stiffness in the cross-links this cannot actually occur. The segments therefore have to experience an extra bending contribution induced by cross-link rotations ($-\Delta\phi$) that restore the angles to their original values. In the parameter regime $y \ll 1$, where bending is the stiffer mode, we therefore expect strong contributions to the energy from the bending mode already in the affine reference state. Allowing furthermore for the relaxation of the smallest segments from their stretched state to even stronger reduce the amount of stretching we might find an exponent as low as $z = 0.07$ not too surprising. In fact, the single filament picture developed above suggests that both deformation modes may be idealized by

springs acting in parallel. Any deformation must necessarily lead to the excitation of both modes, the stiffer of which will contribute most to the elastic energy. In the limit just considered this would lead to $G \propto k_{\perp}$ and to an exponent $z = 0$.

E. Universal Regime

By increasing y from its small value we soften the bending mode and therefore reduce the influence of the fixed cross-link angles on the elastic energy. At the same time the non-affinity scale $l_c \propto y^{1/2}$ increases, indicating ever stronger deviations from the affine reference state.

When, eventually, $l_c \approx l_p \approx \bar{l}_s$ ($\lambda_c \approx y \approx 1$) the affine strain field does not serve as a reference configuration any more, since it is strongly perturbed by a majority of segments with $l_s < l_c$.

At this stage, the two branches, present in the cross-link dominated regime, merge and one enters a universal filament-dominated regime. There, the specific properties of the cross-links do not influence the macroscopic elasticity notably.

While the scaling argument presented for the hinged network ceases to be applicable, the remaining residual forces δf continue to lead to a redistribution of stresses from shorter to longer segments, albeit at higher scales. As we have shown in [30], eventually about 90% of the energy is stored in the longest 30% of the segments only.

The new feature as compared to the regime CL_{free} is that unloading of a segment from its stretched configuration will also lead to stretching of its immediate neighbor on the *same* filament. This way, the available energy for bending of the *crossing* filament, which was the primary contribution in Eq. (23), is reduced. In the limit $y \gg 1$ we can neglect these contributions and calculate the energy from the segments' stretching stiffness only. Being left with one deformation mode only, this necessarily gives a modulus $G \propto \bar{k}_{\parallel}$ and an exponent $z = 1$ as in the affine regime at low densities. However, by resolving the effects according to segment length, we find that the contribution to the total energy grows as $W(l_s) \propto l_s^4$. This strong increase is in accord with the assumption of a large non-affinity scale, below which no energy is stored. While the affine theory considers a single segment only, the physical picture here is that of a serial connection of infinitely many segments along the polymer backbone.

For the network with the fixed cross-link angles one can take the two limiting cases ($y \ll 1, y \gg 1$) together and formally write for the modulus

$$G = a\bar{k}_{\perp} + b\bar{k}_{\parallel}, \quad (27)$$

which nicely contrasts with Eq.(8) derived for cellular materials. In the cellular architecture we have seen that the necessary deformation can be drawn from either mode and it is the softer one that gives the main contribution to the modulus. Here, we find that the presence of infinitely long filaments leads to deformations of bending

as well as stretching nature, in which case it is obvious that the stiffer mode will dominate the energy.

V. CONCLUSION

We have studied the macroscopic elastic properties of networks of semiflexible polymers. We provide exhaustive numerical studies supplemented by scaling arguments that elucidate the subtle interplay between the architecture of the network and the elastic properties of its building blocks to effectuate the macroscopic elasticity.

The main conclusion to be drawn is that, irrespective of the specific architecture chosen, thermally fluctuating stiff polymer networks are inherently more sensitive to polydispersity and randomness than their purely mechanical counterparts. The actual consequences of this susceptibility in terms of the macroscopic elasticity is, on the contrary, highly contingent on the properties of the particular structure. A precise knowledge of the microstructure is therefore indispensable for the interpretation of experimental data.

We have described how the polymer length l_f can be used to drive the system from a simple cellular structure with filaments as short as the mesh-size $l_f \approx \bar{l}_s$, to a fully scale-invariant fibrous structure characterized by infinitely long filaments $l_f \rightarrow \infty$. Especially the latter limit allows for intricate scaling behaviour that impressively demonstrates the qualitative difference between thermally fluctuating and purely mechanical elastic networks.

The elasticity of a simple cellular structure may be described by a serial connection of their elementary deformation modes bending and stretching, respectively. In fibrous networks we have shown that the modes rather act as if they were springs connected in parallel. The network elasticity is therefore always dominated by the stiffer mode, qualitatively similar to a triangulated network, where the specific geometry of the unit cell always imposes stretching deformations on the system, no matter how soft the bending mode actually is. The mechanism leading to this suppression in the fibrous architecture is, in contrast to the local unit-cell effect, highly nonlocal and relies on the action of the whole filament.

Allowing the filaments to freely rotate at the cross-links, a situation which may be highly relevant for F-actin networks cross-linked for example with α -Actinin, we also find an asymptotic scaling regime where stretching and bending modes contribute equally to the elas-

tic energy. By quantifying the degree of co-operation between neighbouring elements in the network we were able to identify a non-affinity length-scale l_c below which the state of affine deformations is rendered unstable. A scaling argument is supplied that allows the calculation of the effective macroscopic exponents starting from this microscopic picture.

It seems that the effects described above can only be accounted for by going beyond the conventional approach that considers *typical polymer segments* only. Instead, we propose to describe the elasticity in terms of a *typical polymer filament* and the spatial distribution of cross-links along its backbone. By controlling the architecture of the network, the scale of the polymer length l_f therefore seems to implicitly influence the elastic properties of the system even in parameter regions where it does not enter the macroscopic elastic moduli explicitly.

Acknowledgments

We gratefully acknowledge fruitful discussions with Oskar Hallatscheck and Klaus Kroy.

APPENDIX A: STIFFNESS MATRIX

The differential equation governing the bending of a beam of length l is given by $X^{(4)} = 0$, with forces F_0, F_l and torques M_0, M_l acting on both ends. The solution can then be written as

$$X(s) = X_0 + X'_0 s + \frac{s^2}{2\kappa} (M_0 - sF_0/3), \quad (A1)$$

while equilibrium conditions require that

$$F_l = -F_0, \quad M_l = -(M_0 - F_0 l). \quad (A2)$$

Stretching the beam is governed by the equation

$$Z(s) = Z_0 + s - \frac{s}{EA} T_0, \quad (A3)$$

with the condition

$$T_l = -T_0 \quad (A4)$$

The four Eqs. (A1), (A2), (A3) and (A4) can now be inverted to yield the forces in terms of the displacements at the beam ends (cross-links)

$$\begin{pmatrix} F_0 \\ T_0 \\ M_0 l \\ F_l \\ T_l \\ M_l l \end{pmatrix} = \frac{\kappa}{l^3} \begin{pmatrix} -12 & 0 & -6 & 12 & 0 & -6 \\ 0 & \Lambda & 0 & 0 & -\Lambda & 0 \\ -6 & 0 & -4 & 6 & 0 & -2 \\ 12 & 0 & 6 & -12 & 0 & 6 \\ 0 & -\Lambda & 0 & 0 & \Lambda & 0 \\ -6 & 0 & -2 & 6 & 0 & -4 \end{pmatrix} \cdot \begin{pmatrix} X_0 \\ Z_0 \\ X'_0 l \\ X_l \\ Z_l \\ X'_l l \end{pmatrix}, \quad (\text{A5})$$

where we have defined $\Lambda = l^2 A/I = 4(l/r)^2$. The second equality only holds for circular beam cross-sections, where the moment of area $I = \pi r^4/4$. The corresponding matrix is called the stiffness matrix.

If, in addition to Eq.(A3), we assume that the stretching response is governed by that of a thermally fluctuating stiff polymer we have to take into account k_{\parallel} of Eq.(4). This is achieved by letting both stretching modes

act in series and substitute $k_s^{-1} \rightarrow k_s^{-1} + k_{\parallel}^{-1}$. Equivalently, one can assign an effective polymer radius

$$r_{pol}^2 = r^2 + \frac{4L^3}{\zeta l_p}, \quad (\text{A6})$$

which now depends on the polymer length as well as on the persistence length l_p of the polymer.

[1] T. Odijk, *Macromolecules* **16**, 1340 (1983).
[2] W. Helfrich and W. Harbich, *Chem. Scr.* **25**, 32 (1985).
[3] B. Hinner *et al.*, *Phys. Rev. Lett.* **81**, 2614 (1998).
[4] H. Isambert and A. C. Maggs, *Macromolecules* **29**, 1036 (1996).
[5] D. Rodney, M. Fivel, and R. Dendievel, *Phys. Rev. Lett.* **95**, 108004 (2005).
[6] S. R. Williams and A. P. Philipse, *Phys. Rev. E* **67**, 51301 (2003).
[7] A. P. Philipse, *Langmuir* **12**, 1127 (1996).
[8] I. Borukhov, R. F. Bruinsma, W. M. Gelbart, and A. J. Liu, *PNAS* **102**, 3673 (2005).
[9] A. G. Zilman and S. A. Safran, *Europhys. Lett.* **63**, 139 (2003).
[10] K. Kroy and E. Frey, *Phys. Rev. Lett.* **77**, 306 (1996).
[11] D. Weaire and S. Hutzler, *The physics of foams* (Oxford University Press, Oxford, 2001).
[12] L. J. Gibson and M. F. Ashby, *Cellular Solids: Structure and Properties* (Cambridge University Press, Cambridge, 1999).
[13] A. M. Kraynik and W. E. Warren, in *Low density cellular plastics*, edited by H. Hilyard and C. Cunningham (Kluwer Academic Publisher, Amsterdam, 1994), Chap. 7.
[14] H. X. Zhu, J. F. Knott, and N. J. Mills, *J. Mech. Phys. Solids* **45**, 319 (1997).
[15] M. J. Silva, W. C. Hayes, and L. J. Gibson, *Int. J. Mech. Sc.* **37**, 1161 (1995).
[16] H. X. Zhu, J. R. Hobdell, and A. H. Windle, *Acta mater.* **48**, 4893 (2000).
[17] A. Fazekas, R. Dendievel, L. Salvo, and Y. Bréchet, *Int. J. Mech. Sc.* **44**, 2047 (2002).
[18] D. Boal, *Mechanics of the Cell* (Cambridge University Press, Cambridge, 2002).
[19] R. Tharmann, M. M. A. E. Claessens, and A. R. Bausch, submitted.
[20] J. H. Shin *et al.*, *PNAS* **101**, 9636 (2004).
[21] O. Kallmes and H. Corte, *Tappi* **43**, 737 (1960).
[22] J. A. Åström, J. P. Mäkinen, M. J. Alava, and J. Timonen, *Phys. Rev. E* **61**, 5550 (2000).
[23] J. A. Åström, S. Saarinen, K. Niskanen, and J. Kurkijärvi, *J. Appl. Phys.* **75**, 2383 (1994).
[24] M. Latva-Kokko and J. Timonen, *Phys. Rev. E* **64**, 2001 (2001).
[25] S. Heyden, Ph.D. thesis, Lund University, 1996.
[26] E. Frey, K. Kroy, J. Wilhelm, and E. Sackmann, in *Dynamical Networks in Physics and Biology*, edited by G. Forgacs and D. Beysens (Springer, Berlin, 1998), Chap. 9.
[27] J. Wilhelm and E. Frey, *Phys. Rev. Lett.* **91**, 108103 (2003).
[28] D. A. Head, A. J. Levine, and F. C. MacKintosh, *Phys. Rev. Lett.* **91**, 108102 (2003).
[29] D. A. Head, A. J. Levine, and F. C. MacKintosh, *Phys. Rev. E* **68**, 61907 (2003).
[30] C. Heussinger and E. Frey, *Phys. Rev. Lett.* in press.
[31] F. C. MacKintosh, J. Käs, and P. A. Janmey, *Phys. Rev. Lett.* **75**, 4425 (1995).
[32] R. L. Satcher and C. F. Dewey, *Biophys. J.* **71**, 109 (1996).
[33] C. Storm *et al.*, *Nature* **435**, 191 (2005).
[34] M. L. Gardel *et al.*, *Science* **304**, 1301 (2004).